# Transport and Elastic Scattering Times as Probes of the Nature of Impurity Scattering in Single-Layer and Bilayer Graphene

M. Monteverde,[1] C. Ojeda-Aristizabal,[1] R. Weil,[1] K. Bennaceur,[2] M. Ferrier,[1] S. Guéron,[1] C. Glattli,[2] H. Bouchiat,[1] J. N. Fuchs,[1] and D. L. Maslov[1,3]

[1]*LPS, Université Paris-Sud, CNRS, UMR 8502, F-91405 Orsay Cedex, France*
[2]*Service de Physique de l'Etat Condensée/IRAMIS/DSM (CNRS URA 2464), CEA Saclay, F-91191 Gif-sur-Yvette, France*
[3]*Department of Physics, University of Florida, Gainesville, Florida 32611, USA*

(Received 19 March 2009; published 26 March 2010)

Transport and elastic scattering times, $\tau_{\rm tr}$ and $\tau_e$, are experimentally determined from the carrier density dependence of the magnetoconductance of monolayer and bilayer graphene. Both times and their dependences on carrier density are found to be very different in the monolayer and the bilayer. However, their ratio $\tau_{\rm tr}/\tau_e$ is found to be close to 1.8 in the two systems and nearly independent of the carrier density. These measurements give insight on the nature (neutral or charged) and range of the scatterers. Comparison with theoretical predictions suggests that the main scattering mechanism in our samples is due to strong (resonant) scatterers of a range shorter than the Fermi wavelength, likely candidates being vacancies, voids, adatoms or short-range ripples.

DOI: 10.1103/PhysRevLett.104.126801 PACS numbers: 73.21.Ac, 73.23.Hk

Since the discovery of the fascinating electronic properties of graphene [1] due to its electronic spectrum with linear dispersion and a perfect electron-hole symmetry at the Fermi level [2], the nature of defects has been shown to play an essential role in determining the carrier density ($n_c$) dependence of the conductance. The wave vector and energy dependences of the impurity potential are known to determine the characteristic scattering times of the carriers. It is important to distinguish the transport time $\tau_{\rm tr}$, which governs the current relaxation and enters the Drude conductivity ($\sigma$), from the elastic scattering time $\tau_e$, which is the lifetime of a plane wave state [3]. Since $\tau_{\rm tr}$ and $\tau_e$ involve different angular integrals of the differential cross section, they differ as soon as the Fourier components of the potential depend on the wave vector $q$. A large ratio $\tau_{\rm tr}/\tau_e$ indicates that scattering is predominantly in the forward direction, so that transport is not affected much by this type of scattering. This is the case in 2D electron gases (2DEG) confined to GaAs/GaAlAs heterojunctions with the scattering potential produced by remote charged Si donors [4], where $\tau_{\rm tr}/\tau_e$ is found to be larger than 10.

The nature of the main scattering mechanism limiting the carrier mobility in graphene is still subject to controversy. It has indeed been shown [5–7] that "white noise" ($q$ independent) scattering leads to a weak (logarithmic) dependence of $\sigma(n_c)$, in contradiction with experiments which typically find a linear increase. In contrast, scattering on charged impurities originates from a $q$ dependent screened Coulomb potential described in the Thomas-Fermi approximation [8–10]. This leads to a linear $\sigma(n_c)$ both for a monolayer (ML) and a moderately doped bilayer (BL). Recent experiments performed to probe this question measured the change in $\sigma$ upon immersion of graphene samples in high-$K$ dielectric media. Their conclusions differ [11]. Alternate explanations involve resonant scattering centers with a large energy mismatch with the Fermi energy of carriers [7,12].

In order to gain insight into the scattering mechanism in graphene, we have extracted $\tau_e$ and $\tau_{\rm tr}$ from magnetotransport in monolayer and bilayer graphene samples. In high magnetic field, when the cyclotron frequency is larger than $1/\tau_e$, the magnetoconductivity exhibits Shubnikov–de Haas (ShdH) oscillations related to the formation of Landau levels. The broadening of these levels at low temperature yields $\tau_e$, while the low-field quadratic magnetoconductivity yields $\tau_{\rm tr}$.

The samples were fabricated by exfoliation of natural graphite flakes and deposition on a doped silicon substrate with a 285 nm thick oxide. The carrier density can be tuned from electrons to holes through the charge neutrality point by applying a voltage on the backgate. The ML and BL samples were identified using Raman spectroscopy. The electrodes were fabricated by electron beam lithography and either sputter deposition of 40 nm thick palladium (samples $A$ and $B$), or Joule evaporation of a bilayer 5 nm Ti/70 nm Au (other samples $C$, $D$, and $E$). We mostly discuss samples $A$ and $B$, a ML and a BL of respective dimensions $W = 1.6\ \mu$m, $L = 1.3\ \mu$m and $W = 4.8\ \mu$m, $L = 0.7\ \mu$m, where $L$ is the distance between the voltage probes covering nearly the entire sample width $W$ (see Fig. 1). The contact resistances were measured to be $20\Omega$ for the BL and calculated to be $200\Omega$ for the ML, and were subtracted. The gate voltage $V_g$ dependence of $\sigma$ is shown for both samples for a range of magnetic fields in Fig. 1. At zero field, one observes a slightly sublinear increase of the conductance on both sides of its minimum at the neutrality point. The mobility varies between 3000 and 5000 $\rm cm^2\,V^{-1}\,s^{-1}$ for the ML, 3000 and 6000 $\rm cm^2\,V^{-1}\,s^{-1}$ for the BL. Above 2 T, steps in the conductance of the ML occur near quantized values

 

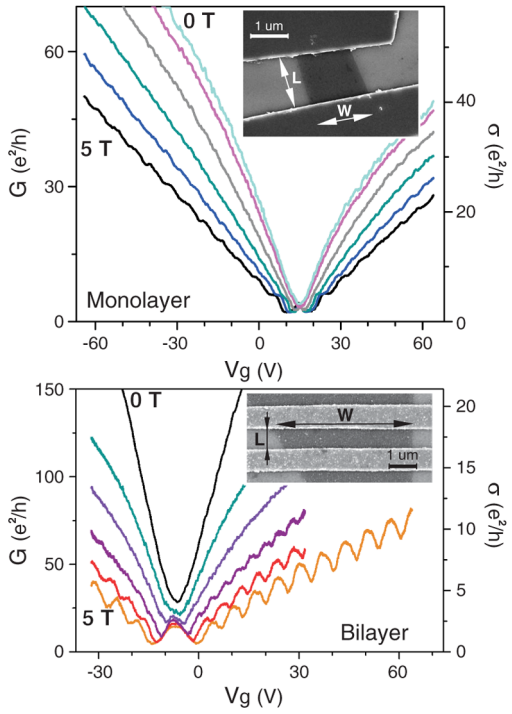


FIG. 1 (color online). Gate voltage dependence of the conductance at several magnetic fields, 1 $T$ apart. The contact resistances have been subtracted. Top panel: monolayer $A$. Bottom panel: bilayer $B$. Inset: electron micrographs of the samples.

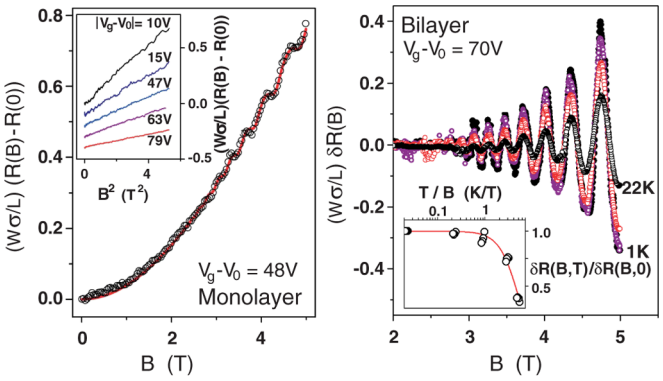


FIG. 2 (color online). Analysis of the magnetoresistance. Left panel: Magnetoresistance of monolayer sample $A$. Dots: experimental points at $T = 1$ K; Continuous line: fit according to Eqs. (2) and (1). Inset: $B^2$ dependence of the low-field magnetoresistance for different gate voltages (Curves shifted along the $Y$ axis for clarity). $\tau_{\rm tr}$ is extracted from the slopes of these curves according to Eq. (2). Notice that the slope increases in the vicinity of the Dirac point reflecting the divergence of the inverse effective mass. Right panel: ShdH oscillations of the longitudinal component of the resistivity in bilayer sample $B$ for different temperatures after subtraction of the quadratic background. The Fermi wave vector $k_F$ and the elastic time $\tau_e$ are deduced from the period and the decay of the oscillations with $1/B$ at low temperature. Inset: Temperature dependence of the oscillations amplitude normalized to $T = 0$. Solid line: fit according to the Lifshitz-Kosevich formula $D_T = \gamma/\sinh(\gamma)$ with $\gamma = 2\pi^2 k_B T/\hbar\omega_c$ [15]. The effective mass determined from this fit is $m_{\rm eff} = 0.035 \pm 0.002 m_e$ in the whole range of gate voltage investigated.

$4(n + 1/2)e^2/h$, as expected. The oscillations in the BL (with a maximum of conductance at the neutrality point) look more unusual but can be understood given the aspect ratio of the sample (see below).

We now describe how we extract $\tau_{\rm tr}$ and $\tau_e$ from the magnetoresistance (MR) (see Fig. 2). The two-terminal MR results from mixing of the diagonal ($\rho_{xx}$) and off-diagonal ($\rho_{xy}$) components of the resistivity tensor [13,14]. The degree of mixing depends on the aspect ratio of the sample. For a square geometry, close to that of the monolayer, $R(B) = [\rho_{xx}^2 + \rho_{xy}^2]^{1/2}$, in a short wide sample such as the bilayer $R(B) = (L/W)[\rho_{xx}^2 + \rho_{xy}^2]/\rho_{xx}$. Intermediate geometries can be calculated following the model developed in [13]. It is then possible to reconstruct the complete MR from the expressions of the resistivity tensor [15] valid in the limit of moderate magnetic field where ShdH oscillations can be approximated by their first harmonics:

$$\delta\rho_{xx}(B)/\rho_0 = 4D_T \exp\left[-\frac{\pi}{\omega_c\tau_e}\right]\cos\left[\frac{j\pi E_F}{\hbar\omega_c} - \phi\right], \quad (1)$$
$$\rho_{xy}(B) = \rho_0\omega_c\tau_{\rm tr} - \delta\rho_{xx}(B)/2\omega_c\tau_{\rm tr},$$

where $\rho_0 = 1/\sigma$ is the zero-field resistivity and $\omega_c = eB/m^*$ is the cyclotron frequency, $m^* = \hbar k_F/v_F$ is the cyclotron mass which depends explicitly on the Fermi wave vector $k_F$ for the ML (constant Fermi velocity). On the other hand, the bilayer's dispersion relation is parabolic at low energy and $m^*$ can be approximated by the effective mass $m_{\rm eff} = 0.035 m_e$, nearly independent of the carrier density in the range of $V_g$ explored where $|E_F| \leq 80$ meV is smaller by a factor of 5 than the energy band splitting [1]. This value of $m_{\rm eff}$ is confirmed by the analysis of the temperature dependence of ShdH oscillations [16]. The phase $\phi$, either $\pi$ or $2\pi$, and the parameter $j$, either 1 or 2, depend on the nature of the sample (ML or BL). The Fermi energy $E_F$ is $\hbar k_F v_F$ for the monolayer and $\hbar^2 k_F^2/(2m_{\rm eff})$ for the bilayer. The prefactor $D_T = \gamma/\sinh(\gamma)$ with $\gamma = 2\pi^2 k_B T/\hbar\omega_c$ describes the thermal damping of the oscillations.

To analyze the data we first deduce $k_F$ from the periodicity of the ShdH oscillations function of $1/B$. We think that this determination is more reliable close to the neutrality point where the sample is possibly inhomogeneous than the estimation of $n_c = k_F^2/\pi$ from the gate voltage and the capacitance between the doped silicon substrate and the graphene sample [17]. Knowing $k_F$ we then determine $\tau_{\rm tr}$ from the quadratic low-field magnetoresistance which is found to be independent of temperature between 1 and 4 K:

$$R(B) - R(0) = \frac{h}{2e^2}\frac{L}{W}\frac{1}{k_F v_F \tau_{\rm tr}}\alpha_g(\omega_c\tau_{\rm tr})^2. \quad (2)$$

We have used the relation $\sigma = \rho_0^{-1} = (2e^2/h)k_F v_F \tau_{\rm tr}$. The dimensionless coefficient $\alpha_g$, which depends on the aspect ratio of the sample, is determined numerically following [13] and the experimental values of $W$ and $L$. It is

found equal to $0.53 \pm 0.01$ and $0.84 \pm 0.02$ for our ML and BL samples $A$ and $B$, respectively. It is important to note that this determination of $\tau_{\rm tr}$ is independent of any assumption of the contact resistance on our two-terminal samples. We finally extract $\tau_e$ from the damping of the first harmonic of ShdH oscillations in the resistivity tensor in $\exp(-\beta/B)$ where $\beta = \pi\hbar k_F/e v_F \tau_e$, see Eq. (1).

The $k_F$ dependences of $\tau_{\rm tr}$ and $\tau_{\rm tr}/\tau_e$ are shown in Fig. 3 for samples $A$ and $B$ as well as three other ML samples, consisting of another two-terminal sample $C$ (very similar to $A$) and two multiterminal samples ($D$ and $E$) with Hall-bar geometry (see [18] for more details). We observe different behaviors for the ML samples, where $\tau_{\rm tr}$ has a minimum at the CNP, and the BL, where it has a maximum. In all cases, despite rather large variations of $\tau_{\rm tr}$, $\tau_{\rm tr}/\tau_e$ is nearly independent of $k_F$. It is equal to $1.7 \pm 0.3$ for the monolayers $A$, $C$, $E$ and to $1.8 \pm 0.2$ for the bilayer in the whole range explored, which corresponds to $n_c$ between $1.5 \times 10^{11}$ and $5 \times 10^{12}$ cm$^{-2}$. That $\tau_{\rm tr}/\tau_e$ is of the order but smaller than 2 indicates that the typical size of the scatterers does not exceed the Fermi wavelength. We note, however, that sample $D$ exhibits a value of $\tau_{\rm tr}/\tau_e$ at high electron doping which is larger than 2 ($\simeq$2.4). The area of this sample (12 $\mu$m$^2$) is much larger than the area ($\simeq 1$ $\mu$m$^2$) of all the other samples $A$, $B$, $C$, and $E$. We suspect that this large sample contains more spatial inhomogeneities than the other smaller samples which could explain a reduced value of $\tau_e$.

Finally, it is also possible to fit $\sigma(V_g)$ at 5 T depicted in Fig. 1 using the value of $\tau_e$ determined as described above.

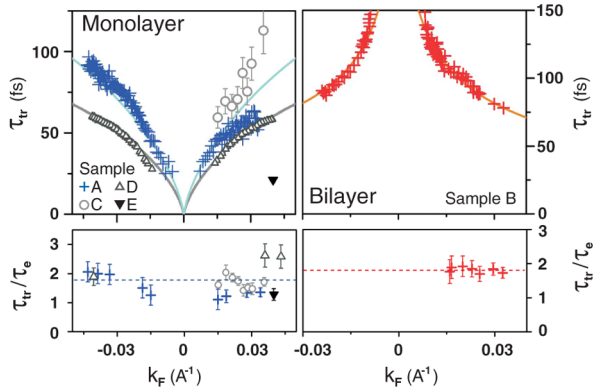


FIG. 3 (color online). $k_F$ dependence of $\tau_{\rm tr}$ and $\tau_{\rm tr}/\tau_e$ ratio. Left panel: monolayers $A$, $C$, $D$, and $E$. Right panel: bilayer $B$. The continuous lines are the fits for samples $A$, $B$, and $D$ according to the resonant impurity model, Eq. (5). For samples $A$ $B$ and $C$ (two-terminal configuration) $\tau_{\rm tr}$ was extracted from the low-field magnetoresistance (crosses), whereas it was extracted from the zero-field conductivity for samples $D$ and $E$. Positive (negative) values of $k_F$ correspond to electron (hole) doping. Lower panels: ratio $\tau_{\rm tr}/\tau_e$ where $\tau_e$ is deduced from the fit of the low temperature decay of the ShdH oscillations. Dotted lines figure the average value $\tau_{\rm tr}/\tau_e = 1.8$. Interestingly, although the mobilities and accordingly $\tau_{\rm tr}$ vary substantially from one sample to the other (from 5000 to 800 cm$^2$/V s from samples $A$ to $E$) the ratio $\tau_{\rm tr}/\tau_e$ is similar for all samples.

Taking into account the geometry of samples $A$ and $B$, following [13], one can relate the contributions of the $n$th Landau level to the conductivity tensor, $\delta_n\sigma_{xx}$ and $\delta_n\sigma_{xy}$ within the semicircular model.

$$\delta_n\sigma_{xx} \sim \exp[-\ln 2(\nu - (\nu_n + \nu_{n+1})/2)/\Gamma_\nu]^2,$$
$$(\delta_n\sigma_{xx})^2 + (\delta_n\sigma_{xy} - \sigma^0_{xy,n})(\delta_n\sigma_{xy} - \sigma^0_{xy,n+1}) = 0. \quad (3)$$

Here, $\nu_n$ is the filling factor of the $n$th level, $\nu$ is the filling factor in between the $n$th and $(n+1)$th levels, and $\sigma^0_{xy,n}$ is the quantized Hall conductivity at the $n$th plateau equal to $4(n+1/2)e^2/h$ and $4ne^2/h$ for the ML and BL, respectively. The width of Landau levels function of filling factor $\Gamma_\nu$ and energy $\Gamma_E = \hbar\sqrt{2\omega_c/\pi\tau_e}$ [19] are related via

$$\Gamma_\nu = \Gamma_E \frac{2}{\hbar v_F}\sqrt{\frac{\nu_n \Phi_0}{\pi B}}. \quad (4)$$

Good agreement between the experimental data and the two-terminal $G(V_g)$ of the ML, calculated from the conductivity tensor [13,14], is obtained taking the filling factor dependence of $\Gamma_\nu$ from Eq. (4); see Fig. 4. For the BL, we had to modify the semicircular relation in a similar way as done in Ref. [14].

We now compare our results on $\tau_e$ and $\tau_{\rm tr}$ to recent theoretical predictions. We first consider scattering on charged impurities [8,9]. In particular, the question of the difference between $\tau_e$ and $\tau_{\rm tr}$ has been addressed for a graphene monolayer [20]. The minimum value of the ratio $\tau_{\rm tr}/\tau_e$ is obtained when the impurities are located close to the graphene foil, in which case it is expected to be 2—as a result of the absence of backscattering—and independent of $n_c$. This is a bit larger than the measured ratio for most samples. Screened charged impurities are characterized by a screening radius $1/q_{\rm sc}$, which in the Thomas-Fermi approximation is given by $1/q_{TF} \equiv \pi\epsilon\hbar v_F/e^2 k_F$, where

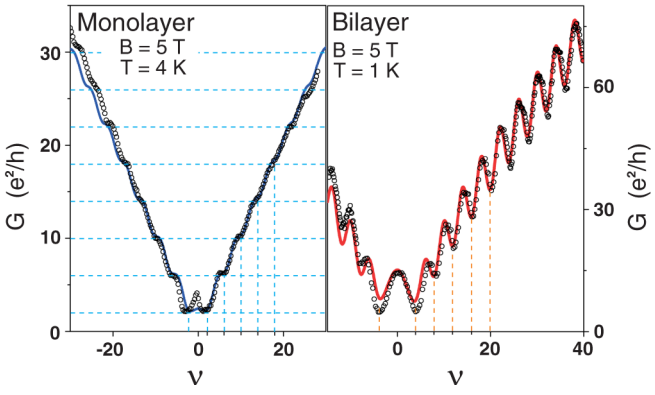


FIG. 4 (color online). Comparison of $G(\nu)$ at 5 T for samples $A$ and $B$ with the expression of the conductance derived in Ref. [13], taking the aspect ratio $L/W$ of each sample and using Eqs. (3) and (4) with $\tau_e(k_F)$ determined above. The dashed vertical lines indicate the positions of $\nu_n$ which, as expected, are different for the mono $\nu_n = \pm 4(n+1/2)$ and the bilayer $\nu_n = \pm 4n$. The conductance quantization is well obeyed for the monolayer but not for the bilayer. This is well explained by the aspect ratio of the bilayer sample [13,14].

$\epsilon$ is the appropriate dielectric constant. In the Born approximation, the transport time is $\tau_{\rm tr} \propto q_{\rm sc}^2 v_F/k_F$. For a monolayer, $q_{TF}/k_F$ is a constant $\simeq 3$ and both $\tau_{\rm tr}$ and $\tau_e$ are then expected to increase as $k_F$, which is not what we observe in Fig. 3 where the increase is sublinear. The disagreement is even stronger for a bilayer, where the ratio $q_{TF}/k_F \propto 1/k_F$ varies between 3 at high doping and 12 close to the neutrality point. The transport time is then expected to vary linearly with $n_c$, if the screening radius is estimated as $\sim 1/k_F$, or to be independent of $k_F$ if estimated as $\sim 1/q_{TF} \ll 1/k_F$ [9], neither of which agrees with our data; see Fig. 3.

An alternative explanation is resonant scattering resulting from vacancies or any other kind of impurities of range $R$ such that $a \lesssim R \ll 1/k_F$, where $a$ is the carbon-carbon distance, and with a large potential energy [7,12]. It is characterized by a transport cross section

$$A_{\rm tr} \simeq \frac{\pi^2}{k_F \ln^2(k_F R)}. \quad (5)$$

The resulting transport time $\tau_{\rm tr} = 1/(n_i v_F A_{\rm tr})$ ($n_i$ is the concentration of impurities) leads to a conductance increasing as $n_c$ with logarithmic corrections for both the ML and BL. In both cases, our extracted $\tau_{\rm tr}(k_F)$ (see Fig. 3) are compatible with the square logarithmic dependence of Eq. (5). It is also possible to estimate the range of the impurity potential 0.5 Å $\leq R \leq$ 2.5 Å and the concentration of impurities $n_i = (8 \pm 2) \times 10^{11}$ cm$^{-2}$, which turns out to be identical for samples $A$ and $B$. This is of the order of the minimum value of the carrier density $n_{\rm min} = 1.5 \times 10^{11}$ cm$^{-2}$, extracted from the experiment. It is also interesting to note that the minimum conductivity expected for this resonant impurity model, $\sigma_{\rm min} = (2e^2/\pi h) \times (n_{\rm min}/n_i) \ln^2(R\sqrt{\pi n_{\rm min}}) = 3.7 e^2/h$ and $4.5 e^2/h$ for the ML and the BL, respectively, are similar to the observed experimental values which are 3.3 and $4.1 e^2/h$. This analysis also corroborates our results on the ratio $\tau_{\rm tr}/\tau_e$ indicating scatterers with a range smaller than the Fermi wavelength (but possibly of the order of or slightly larger than the lattice spacing). Whereas the resonant character is not essential for the validity of Eq. (5) for massive carriers (corresponding to the bilayer) [21], it has been shown that it is essential for massless carriers in the monolayer [22]. This resonantlike character, although not straightforward, has been demonstrated in the case of scattering centers created by vacancies in graphene over a wide range of Fermi energies [23]. As shown in detail in [18], it is not necessary to fine-tune $k_F$ to obtain the $\ln^2$ dependence in Eq. (5).

In conclusion, our results indicate that the main scattering mechanism in our graphene samples is due to strong neutral defects, with a range shorter than the Fermi wavelength and possibly of the order of $a$, inducing resonant (but not unitary) scattering. Likely candidates are vacancies, as observed recently in transmission electron microscopy [24], voids, adatoms, or short-range ripples as suggested in [25]. This does not exclude the presence of long-range charged impurities responsible for electron-hole puddles but their contribution to the scattering rates $1/\tau_{\rm tr}$ and $1/\tau_e$ appears to be negligible in all the samples investigated.

We thank R. Deblock, M. Goerbig, G. Montambaux, A. Kasumov, and A. Mirlin for fruitful discussions. This work was supported by the EU-STREP program HYSWITCH, and "CEE MEST CT 2004 514307 EMERGENT CONDMATPHYS Orsay," Cnano IdF DYNA, RTRA "Triangle de la Physique, QUANTGRA" grants.

[1] A. H. Castro Neto *et al.*, Rev. Mod. Phys. **81**, 109 (2009).
[2] P. R. Wallace, Phys. Rev. **71**, 622 (1947).
[3] E. Akkermans and G. Montambaux, *Mesoscopic Physics with Electrons and Photons* (University Press, Cambridge, 2007).
[4] P. T. Coleridge, Phys. Rev. B **44**, 3793 (1991).
[5] N. Shon and T. Ando, J. Phys. Soc. Jpn. **67**, 2421 (1998).
[6] I. L. Aleiner and K. B. Efetov, Phys. Rev. Lett. **97**, 236801 (2006).
[7] P. M. Ostrovsky, I. V. Gornyi, and A. D. Mirlin, Phys. Rev. B **74**, 235443 (2006).
[8] K. Nomura and A. H. MacDonald, Phys. Rev. Lett. **96**, 256602 (2006); T. Ando, J. Phys. Soc. Jpn. **75**, 074716 (2006).
[9] S. Adam and S. Das Sarma, Phys. Rev. B **77**, 115436 (2008).
[10] S. Adam, S. Cho, M. Fuhrer, and S. Das Sarma Phys. Rev. Lett. **101**, 046404 (2008).
[11] C. Jang *et al.*, Phys. Rev. Lett. **101**, 146805 (2008); L. A. Ponomarenko *et al.*, Phys. Rev. Lett. **102**, 206603 (2009).
[12] M. I. Katsnelson and K. S. Novoselov, Solid State Commun. **143**, 3 (2007); T. Stauber, N. M. T. Peres, and F. Guinea, Phys. Rev. B **76**, 205423 (2007).
[13] D. A. Abanin and L. S. Levitov, Phys. Rev. B **78**, 035416 (2008).
[14] J. R. Williams *et al.*, Phys. Rev. B **80**, 045408 (2009).
[15] I. M. Lifshitz and A. M. Kosevich, Sov. Phys. JETP **2**, 636 (1956); P. T. Coleridge, R. Stoner, and R. Fletcher, Phys. Rev. B **39**, 1120 (1989).
[16] This yields the BL's effective mass, which agrees with the theoretical value of $2\hbar^2 t_\perp/(9a^2 t_\parallel^2)$, where $t_\parallel$ and $t_\perp$ are the in-plane and transverse hopping energies [1].
[17] S. Cho and M. S. Fuhrer, Phys. Rev. B **77**, 081402(R) (2008).
[18] See supplementary material at http://link.aps.org/supplemental/10.1103/PhysRevLett.104.126801 for a description of samples *C*, *D*, and *E*, and a review on 2D scattering.
[19] T. Ando and Y. Uemura, J. Phys. Soc. Jpn. **36**, 959 (1974).
[20] E. H. Hwang and S. Das Sarma, Phys. Rev. B **77**, 195412 (2008).
[21] S. K. Adhikari, Am. J. Phys. **54**, 362 (1986).
[22] D. S. Novikov, Phys. Rev. B **76**, 245435 (2007).
[23] D. M. Basko, Phys. Rev. B **78**, 115432 (2008).
[24] J. C. Meyer *et al.*, Nano Lett. **8**, 3582 (2008).
[25] F. Guinea, M. I. Katsnelson, and M. A. H. Vozmediano, Phys. Rev. B **77**, 075422 (2008).